Available online at www.sciencedirect.com
SCIENCE DIRECT®
Journal of Catalysis 219 (2003) 310–319
JOURNAL OF CATALYSIS
www.elsevier.com/locate/jcat

On the enhanced *para*-selectivity of HZSM-5 modified by antimony oxide

Shourong Zheng, Andreas Jentys,* and Johannes A. Lercher

Institut für Technische Chemie II, Technische Universität München, Lichtenbergstrasse 4, 85747 Garching, Germany

Received 10 January 2003; revised 12 May 2003; accepted 15 May 2003

Abstract

HZSM-5 was modified with antimony oxide by solid-state reaction at 773 K to enhance diffusional constraints. Crystalline phases of antimony oxide were not detected at a Sb_2O_3 loading up to 10.2 wt%. Antimony oxide was found to strongly interact with the hydroxyl groups of the zeolite, i.e., silanol and bridging hydroxyl groups, and with extra-framework aluminum oxide. Only a small amount of Sb_2O_3 penetrated the pores of the zeolite, while the main fraction of Sb_2O_3 was deposited on the external surface of the zeolite crystals. With increasing antimony oxide loading a pronounced pore narrowing of the zeolite was observed, which suppressed the further penetration of antimony oxide into the pores of the zeolite. The dispersion of antimony oxide on the surface of the zeolite led to complete removal of unselective Brønsted acid sites and to a narrowing/blocking of the pore mouth openings of the zeolite. Both effects induced enhanced *para*-selectivity for toluene disproportionation.

Keywords: Antimony oxide modification; HZSM-5; Passivation of acid sites; Diffusivity; *para*-Selectivity; Toluene disproportionation

1. Introduction

Due to their unique structure HZSM-5 zeolites are *para*-selective catalysts in toluene disproportionation, methylation of toluene, and xylene isomerization [1,2]. Further enhancement of the shape selectivity can be achieved by postsynthetic modification, which leads to removal of unselective acid sites located in the pore mouth regions and/or to a narrowing of the pore openings. This modification of HZSM-5 effectively suppresses the secondary isomerization to undesired *o*- and *m*-xylenes and enlarges the differences in the diffusivities between *o*- or *m*-isomers and *p*-isomer [3–6].

The aim of the postsynthetic modification is to deposit (non)metal oxides on the external surface of zeolite crystals. Niwa et al. [7,8] systematically studied the modification of zeolites by chemical vapor deposition (CVD) and found that amorphous SiO_2 layers were formed on the external surface of the zeolite only if bulky molecules, such as $Si(OCH_3)_4$ and $Si(OC_2H_5)_4$, were used as silylation agents. Tynjala et al. [9] found that the deposition of SiO_2 and Ge_2O_3 by CVD on the surface of zeolites effectively enhanced the selectivity to small olefins and linear aliphatic products in the conversion of methanol to hydrocarbons. Kaeding et al. [10,11] observed an enhanced *para*-selectivity for the alkylation of toluene with methanol on phosphorus-modified HZSM-5 zeolites and suggested that the phosphorus reagent interacted with the acid sites of the zeolite and attached to the zeolite via framework oxygen atoms, which partially blocked the pore openings and, therefore, restricted the diffusion of *m*- and *o*-xylenes. Kaeding et al. [12,13] further studied the modification of HZSM-5 with Ca, Mg, B, and Mn oxides and achieved enhanced *para*-selectivity for toluene methylation and toluene disproportionation.

The deposition of oxides onto the surface of zeolites can be carried out by impregnation [14], ion exchange [15], chemical deposition [7,8,16,17], and solid-state reactions [18,19]. Karge et al. [18] used solid-state reactions to achieve a markedly higher exchange degree of La ions in zeolite Y compared with ion exchange in liquid phase. The ion exchange of Ni and Co into HZSM-5 and zeolite Y was studied by Jentys and co-workers [20,21], who also achieved a significantly higher degree of exchange degree with a solid-state reaction than with ion exchange in liquid phase due to the absence of hydration of the cations in the solid reaction. MoO_3-modified HZSM-5 zeolite obtained by solid-state reaction showed benzene selectivity for the conversion of methane to aromatics similar to that prepared by the impregnation method [22,23]. Xiao et al. [24] observed enhanced conversion over $CuCl_2$/HZSM-5 catalysts

* Corresponding author.
E-mail address: andreas.jentys@ch.tum.de (A. Jentys).

0021-9517/$ – see front matter
doi:10.1016/S0021-9517(03)00234-3

prepared by solid-state reaction for the selective reduction of NO by propylene compared with CuZSM-5 obtained using ion exchange in aqueous phase. Modification of HZSM-5 with antimony oxide by solid-state reaction was studied by Lee et al. [25], who reported enhanced *para*-selectivity of antimony oxide-modified HZSM-5 zeolites for toluene methylation by methanol. Systematic and quantitative studies on the dispersion of oxides and salts on the surface of different supports were comprehensively reviewed by Xie and Tang [19].

In this contribution we describe the interaction between antimony oxide and HZSM-5 zeolite, the location of antimony oxide, and the modification effects using IR spectroscopy, Raman spectroscopy, XRD, and sorption of probe molecules related the structural properties of the modified materials to their activity and shape selectivity in the toluene disproportionation reaction.

2. Experimental

2.1. Materials

HZSM-5 zeolite with a Si/Al ratio of 45 and particle size of 0.5 μm, determined by SEM, was used as the parent material. A series of antimony oxide-modified samples were prepared by heating a physical mixture of antimony oxide and the zeolite under N_2 atmosphere to 773 K at the rate of 10 K/min followed by calcination at this temperature for 2 h. The antimony oxide content of the modified zeolites after calcination was determined by chemical analysis (AAS). Pore volumes of the parent and modified zeolites were measured by N_2 adsorption with a Micrometrics ASAP 2000 apparatus at 77.3 K. XRD patterns of the parent and antimony oxide-modified zeolites were collected in a Philips XRD powder diffraction meter using Cu-K_α radiation and a 2θ scan rate of 10°/min.

2.2. ^{27}Al MAS NMR

^{27}Al MAS NMR spectra of the parent and modified zeolites were recorded on a Bruker AVANCE MSL-300 NMR spectrometer at a field strength of 7.5 T and 15-kHz spinning speed using 4-mm ZrO_2 rotors. Spectra were collected at a frequency of 78.205 MHz with 1.0-μs excitation pulses and 0.1-s recycle times. The ^{27}Al chemical shifts were referenced to a 1 M aqueous solution of $Al(NO_3)_3$.

2.3. In situ Raman and IR spectroscopy

For in situ Raman measurements, the physical mixture of antimony oxide (20 wt%) and the zeolite was pressed into a self-supporting wafer and placed in a sample holder consisting of a gold plate attached to a heating wire. The sample holder was mounted in the center of a Raman cell connected to a flow system. The sample was heated to 873 K (rate of 5 K/min) under a N_2 flow of 20 ml/min. Raman spectra were collected every 2 min with a Renishaw Raman spectrometer (Type 1000) equipped with a CCD detector using a 785-nm diode laser for excitation.

The dispersion of antimony oxide over the zeolite as a function of the calcination temperature was followed using IR spectroscopy. A self-supporting wafer of the physical mixture of antimony oxide (5 wt%) with the zeolite was placed in a gold sample holder in the center of a furnace, which was connected to a vacuo system. The sample was heated in vacuo ($< 10^{-6}$ mbar) to 823 K (rate of 5 K/min) and IR spectra were collected in a time interval of 1 min with 4 cm^{-1} resolution using a Bruker IFS 88 FTIR spectrometer.

2.4. Pyridine and tert-butylpyridine (DTBPy) adsorption

A self-supporting wafer of the sample was placed in a gold sample holder in the center of a furnace, which was connected to a vacuo system. During activation the sample was heated in vacuo ($< 10^{-6}$ mbar) to 773 K at the rate of 10 K/min and kept at this temperature for 1 h. The adsorption of pyridine or DTBPy was carried out at a partial pressure of 2×10^{-2} mbar using an equilibration time of 15 min. After physically adsorbed molecules were removed by outgassing at 423 K for 1 h, IR spectra were collected at 423 K with 4 cm^{-1} resolution using a Bruker IFS 88 FTIR spectrometer. To allow quantitative comparison of the intensities of IR bands, all IR spectra were normalized using the area of the overtones of lattice vibration bands of the zeolites at 1990 and 1870 cm^{-1}.

2.5. Diffusion measurements

The diffusivities of *o*-xylene in the parent and antimony oxide-modified zeolites were determined using IR spectroscopy in a flow system, which was described previously [26,27].

The zeolite was pressed into a self-supported wafer, placed inside a gold sample holder, and mounted in the center of an in situ cell connected to a flow system. The sample was activated in helium flow by heating to 773 K at the rate of 10 K/min and holding at this temperature for 1 h. After the sample temperature was stabilized at 373 K, *o*-xylene with a partial pressure of 1 mbar was injected into carrier gas using a syringe pump. IR spectra were collected in a 30-s interval. The diffusion coefficients were calculated using the square root law [28,29],

$$Q_t/Q_\infty = 6/r_0(Dt/\pi)^{1/2},$$

where Q_t denotes the amount adsorbed at time t (s), Q_∞ is the amount adsorbed at equilibrium coverage, r_0 is the radius of zeolite crystal, and D is the diffusion coefficient.

The area of the IR bands at 1497 and 1468 cm^{-1} was used to quantify the relative amount of *o*-xylene adsorbed in the zeolites. To compare different samples the spectra were nor-

malized to the intensity of the overtone vibration of HZSM-5 at 1990 and 1870 cm^{-1}.

2.6. Toluene disproportionation

Toluene disproportionation was carried out in a fixed-bed reactor at 773 K. Prior to the experiments 0.06 g of sample was activated at 773 K for 1 h in a He stream of 20 ml/min. Toluene was injected into the He stream using a syringe pump. The partial pressure of toluene in the He stream of 20 ml/min was 22.5 mbar. The composition of the products from the toluene disproportionation reaction was analyzed with an on-line gas chromatograph equipped with a flame ionization detector.

3. Results

3.1. Material synthesis and characterization

The antimony oxide content before and after calcination at 773 K and the pore volumes of the parent and modified zeolites are listed in Table 1. Chemical analysis of the modified zeolites showed that the antimony oxide content substantially decreased for all modified samples after calcination at 773 K, suggesting that a significant fraction of antimony oxide was lost during calcination. Modification of the zeolite with 3.3 wt% antimony oxide led to a decrease in the pore volume by 8 rel.%, which is tentatively assigned to filling of parts of the zeolite pores with Sb_2O_3. Further increase in Sb_2O_3 loading did not lead to a decrease in zeolite pore volumes.

XRD patterns of the parent and antimony oxide-modified zeolites are compared in Fig. 1. In the XRD pattern of the parent zeolite only diffraction peaks typical of HZSM-5 were present. In the physical mixture of 5 wt% antimony oxide and zeolite the diffraction peaks of antimony oxide were clearly observed, while after calcination of the mixture at 773 K diffraction peaks assigned to antimony oxide disappeared. Note that crystalline phases of antimony oxide were not detected in any of the modified zeolites after calcination.

In situ Raman spectroscopy was used to study the changes in the crystalline phases of antimony oxide during the solid-state reaction of Sb_2O_3 with the zeolite. Raman spectra of the physical mixture of the parent zeolite and antimony oxide (20 wt%) calcined at different temperatures are shown in Fig. 2. At ambient temperature, bands assigned to antimony oxide were clearly observed at 450, 373, 253, and 189 cm^{-1}. In addition a broadband at low wavenumber resulting from fluorescence effects was observed. With increasing calcination temperature, the intensity of the broadband increased, which is a result of the enhanced fluorescence effects of the dehydrated zeolite due to the formation of surface hydroxyl groups [30]. The intensity of Raman bands assigned to antimony oxide started to decrease at a calcination temperature of 623 K and all bands completely disappeared at a calcination temperature of 723 K, indicating also the absence of crystalline antimony oxide in the mixture after the solid-state reaction.

The changes in concentration of the silanol and bridging hydroxyl groups of the zeolite, followed by in situ IR spec-

Table 1
Antimony oxide content and pore volume of the samples

Code	Sb_2O_3 content (wt%)		Pore volume (cm^3/g)	Corrected pore volume (cm^3/g)[a]
	Before calcination	After calcination		
HZ	–	–	0.088	0.088
SbZ1	5	3.3	0.078	0.081
SbZ2	10	6.5	0.07	0.075
SbZ3	15	7.7	0.07	0.076
SbZ4	20	10.2	0.069	0.077

[a] Corrected based on the content of antimony oxide after calcination.

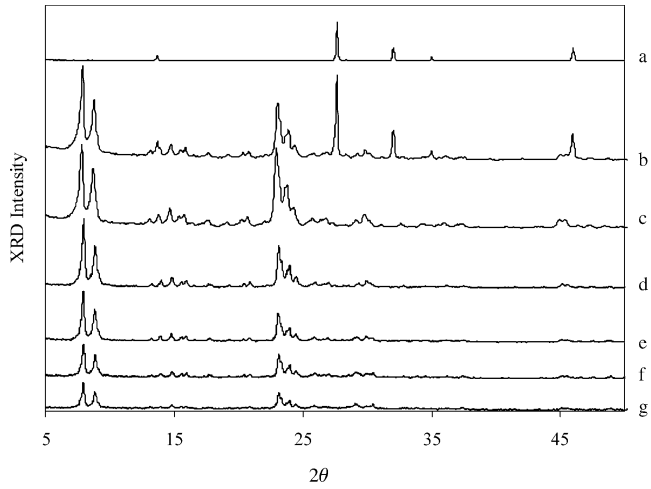

Fig. 1. XRD patterns of (a) antimony oxide, (b) physical mixture of antimony oxide and zeolite, (c) HZ, (d) SbZ1, (e) SbZ2, (f) SbZ3, and (g) SbZ4.

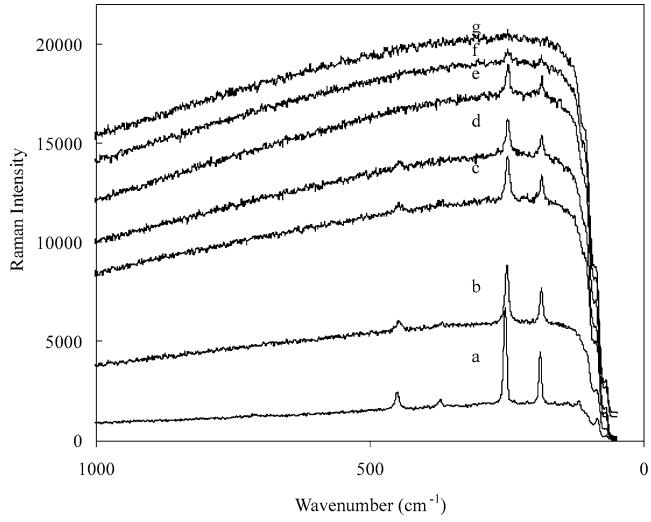

Fig. 2. Raman spectra of the physical mixture of antimony oxide with zeolite calcined at (a) 323 K, (b) 473 K, (c) 573 K, (d) 623 K, (e) 683 K, (f) 703 K, and (g) 723 K

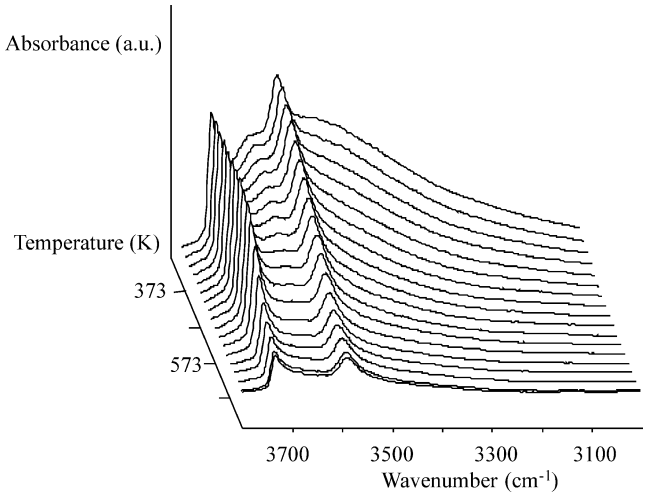

Fig. 3. In situ IR spectra during the solid-state reaction of Sb_2O_3 and HZSM-5.

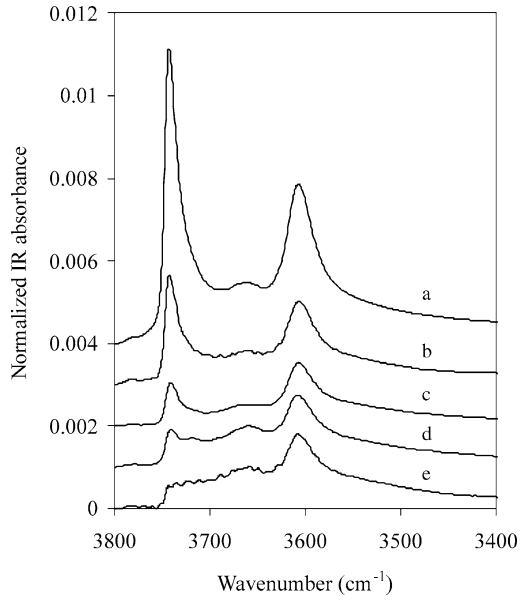

Fig. 4. IR spectra of activated (a) HZ, (b) SbZ1, (c) SbZ2, (d) SbZ3, and (e) SbZ4.

troscopy, showed a similar trend. IR spectra recorded during the solid-state reaction of a physical mixture of the zeolite and Sb_2O_3 (5 wt%) are shown in Fig. 3. At ambient temperature, a broad band around 3000 cm^{-1} and two bands at 3745 and 3606 cm^{-1}, characteristic of the silanol and bridging hydroxyl groups of the zeolite, were observed in the hydroxyl group region. With increasing calcination temperature, the intensity of the broad band continuously decreased, which is attributed to desorption of H_2O. At 643 K, the intensity of the hydroxyl groups decreased continuously, which is an indication of the solid-state reaction between Sb_2O_3 and the zeolite. At temperatures higher than 713 K a further decrease in the intensity of the bands characteristic of the hydroxyl groups was not observed.

Table 2
Changes in the concentration of hydroxyl groups after modification with Sb_2O_3

Sample	Decrease in the concentration (%)	
	Silanol groups	Bridging hydroxyl groups
SbZ1	60	48
SbZ2	87	48
SbZ3	93	50
SbZ4	98	48

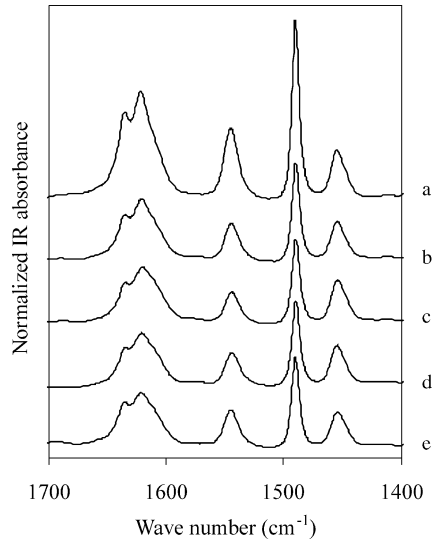

Fig. 5. IR spectra during adsorption of 2×10^{-2} mbar pyridine in (a) HZ, (b) SbZ1, (c) SbZ2, (d) SbZ3, and (e) SbZ4.

IR spectra of the hydroxyl groups of the zeolites after Sb_2O_3 modification are shown in Fig. 4. Three IR bands at 3745, 3680, and 3606 cm^{-1} were observed in the hydroxyl group region, which can be assigned to nonacidic silanol groups, hydroxyl groups of extra-framework aluminum oxide, and bridging hydroxyl groups, respectively [31]. The relative changes in the concentration of the hydroxyl groups are summarized in Table 2.

Modification with 3.3 wt% antimony oxide led to a decrease in the intensity of the silanol groups by 60% and of the bridging hydroxyl groups by 48%, respectively. A slight decrease in the intensity of the hydroxyl groups of the extra-framework aluminum was also observed. A further increase in antimony oxide loading to 6.5 wt% led to a decrease in the intensity of the silanol groups by 87%, while a further decrease in the intensity of the bridging hydroxyl groups was not observed. At 10.2 wt% antimony oxide loading, the silanol groups almost completely disappeared, while the intensity of the bands of the bridging hydroxyl groups was similar to those of all other Sb_2O_3-modified samples.

IR spectra after adsorption of pyridine on the Sb_2O_3 modified samples are shown in Fig. 5. IR bands at 1636, 1490, and 1545 cm^{-1}, characteristic of pyridinium ions (pyridine chemisorbed at Brønsted acid sites), and at 1623, 1490, and 1454 cm^{-1}, characteristic of coordinatively bound

Table 3
Changes in the concentration of acid sites after modification with Sb_2O_3

Sample	Decrease in the concentration (%)	
	Lewis acid sites	Brønsted acid sites
SbZ1	21	51
SbZ2	22	50
SbZ3	18	54
SbZ4	21	48

pyridine (pyridine interacting with Lewis acid sites), were observed [32,33]. The intensity of the bands at 1545 and 1454 cm^{-1} was used to calculate the relative changes in the concentration of acid sites after the modification, which are summarized in Table 3. Note that for all samples investigated the band characteristic of the bridging hydroxyl groups at 3606 cm^{-1} completely disappeared after pyridine adsorption (spectra not shown), which indicates that all bridging hydroxyl groups (strong Brønsted acid sites) were accessible for pyridine and, therefore, a partial blocking of the pores after modification of the zeolites can be excluded. The changes in the concentrations of Lewis and Brønsted acid sites clearly revealed that the modification led to decreases in the concentrations of Lewis and Brønsted acid sites on all modified samples of about 20 and 50%, respectively, which is in perfect agreement with the concentration of hydroxyl groups present after Sb_2O_3 modification.

Sorption of DTBPy was used to quantify the concentration of the externally accessible acid sites. The kinetic diameter of DTBPy (0.7 nm) is significantly larger than the pore openings of HZSM-5 [34–36]. Therefore, this probe molecule can interact only with hydroxyl groups located on the external surface or in the pore mouth region of the zeolite. IR spectra of DTBPy adsorption on the parent and modified zeolites are compiled in Fig. 6.

For the unmodified zeolite, the adsorption of DTBPy led to a marked decrease in the intensity of the bands at 3745 and 3606 cm^{-1} resulting from interaction between the hydroxyl groups and DTBPy molecules. Other bands at 2979, 2943, 2912, and 2882 cm^{-1}, characteristic of interaction of CH_3 groups with hydroxyl groups of the zeolite, at 3367 and 1616 cm^{-1}, characteristic of interaction of DTBPy molecules with Brønsted acid sites, and at 1541, 1481, and 1468 cm^{-1}, characteristic of physically adsorbed DTBPy, were also observed. The bands at 3367 and 1616 cm^{-1}, assigned to the N–H vibration and to the ring vibration of $DTBPyH^+$, respectively [34,35], were used to determine the concentration of externally accessible Brønsted acid sites [36]. Approximately 28% of the bridging hydroxyl groups of the parent zeolite are accessible for DTBPy molecules. After modification of HZSM-5 with 3.3 wt% Sb_2O_3, sorption of DTBPy at room temperature was almost completely suppressed. Only IR bands in the C–H stretching vibration region around 2979 cm^{-1} were observed at very low intensity [34], while the bands at 3367 and 1616 cm^{-1}, characteristic of the interaction of DTBPy molecules with Brønsted acid sites, were absent. After evacuation of the

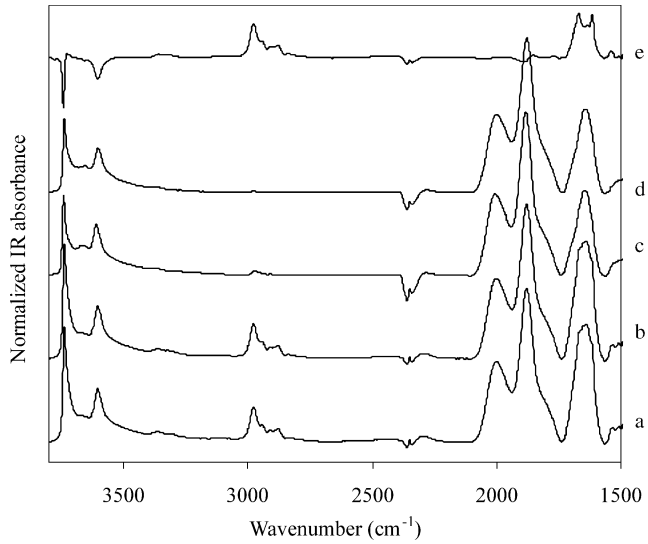

Fig. 6. IR spectra during adsorption of 2×10^{-2} mbar of DTBPy (a) HZ at room temperature, (b) HZ after outgassing at 423 K for 1 h, (c) SbZ1 at room temperature, (d) SbZ1 after outgassing at 423 K for 1 h, and (e) difference spectra of HZ between after desorption and before adsorption of DTBPy.

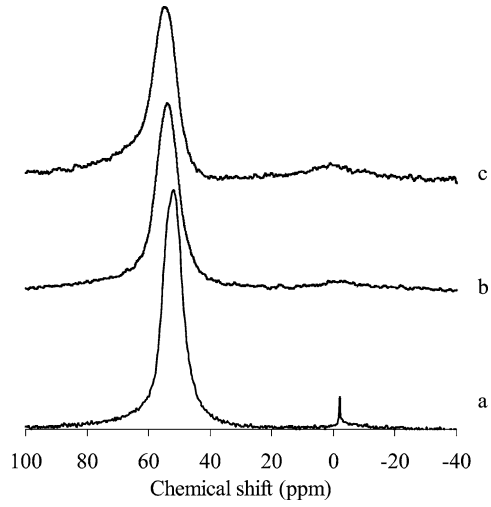

Fig. 7. ^{27}Al MAS NMR spectra of (a) HZ, (b) SbZ1, and (c) SbZ4.

antimony-oxide modified sample at 423 K for 1 h IR bands around 2979 cm^{-1} were completely removed from the surface, indicating that DTBPy molecules were only physically absorbed. Adsorption of DTBPy on the samples with higher Sb_2O_3 loadings gave similar results, which indicates that after the modification all externally accessible Brønsted acid sites of the zeolite were chemically blocked.

^{27}Al MAS NMR spectra of HZ, SbZ1, and SbZ4 are compared in Fig. 7. Two peaks with chemical shifts at 53 and −5 ppm are typically observed for HZSM-5 zeolite, which are assigned to the framework Al (FAL) and extra-framework Al oxide (EFAL) species, respectively. Integration of these peaks in the NMR spectrum of HZ revealed that about 2.5% of the Al was present as EFAL. For both Sb_2O_3-modified samples the intensity of the peak at −5 ppm

decreased and became significantly broadened compared with the parent material, which resulted from the change in the coordination environment of EFAL. This confirms that the decrease in the concentration of the bridging hydroxyl groups observed after solid-state reactions does not result from a partial dealumination, i.e., removal of Al from the T-atom positions of the zeolite. In addition, the marked broadening of the peak of EFAL, e.g., the change in the coordination environment of EFAL, suggests a strong interaction of Sb_2O_3 with EFAL.

3.2. Diffusion of *o*-xylene in parent and modified samples

The diffusion of *o*-xylene (kinetic diameter of 0.63 nm [37]) was used to study the effects of the modification on the pore openings of the zeolite. Typical IR spectra during the time-resolved uptake of *o*-xylene over H-ZSM5 at 373 K are presented in Fig. 8. With increasing adsorption time, the intensity of IR bands at 3745 and 3606 cm^{-1} decreased, indicating interaction of *o*-xylene with the hydroxyl groups via hydrogen bonding, and a broadband around 3168 cm^{-1} characteristic of the perturbed bridging hydroxyl groups. Simultaneously, the intensity of the IR bands assigned to *o*-xylene at 1497, 1468, and around 3000 cm^{-1} increased. The changes in the intensity of the bands at 1497 and 1468 cm^{-1}

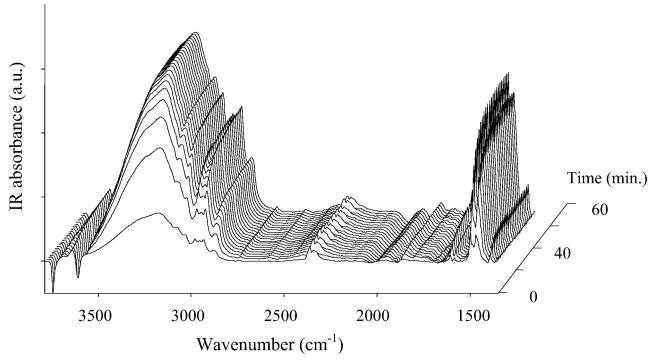

Fig. 8. Time-resolved IR spectra during adsorption of 1 mbar *o*-xylene in HZ at 373 K.

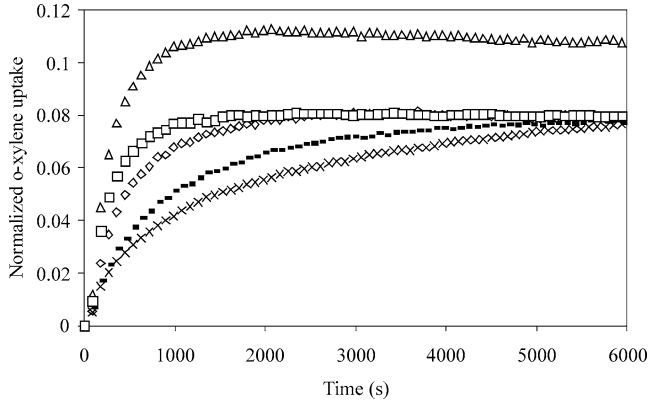

Fig. 9. Intensity of the bands at 149 and 1468 cm^{-1} during *o*-xylene adsorption with 1 mbar at 373 K in (Δ) HZ, (□) SbZ1, (◇) SbZ2, (–) SbZ3, and (×) SbZ4.

Table 4
Diffusion coefficients of *o*-xylene in the parent and modified zeolites

Sample	Diffusion coefficient of *o*-xylene ($\times 10^{-18}$ m^2/s)
HZ	7.8
SbZ1	7.4
SbZ2	3.9
SbZ3	1.9
SbZ4	0.66

as a function of adsorption time over the parent and modified samples are compared in Fig. 9. An equilibration time of 30 min was observed for *o*-xylene adsorption in the unmodified zeolite. After modification with 3.3 wt% Sb_2O_3 a decrease in *o*-xylene uptake by approximately 26% was observed, while the equilibration time of *o*-xylene adsorption was not affected, indicating the same diffusivity as the parent material. A further increase in Sb_2O_3 loading resulted in a marked decrease in *o*-xylene diffusivity; however, the uptake of *o*-xylene remained the same for all modified samples. The diffusion coefficients of *o*-xylene in the parent and modified zeolites, calculated using the square root law, are listed in Table 4.

For the parent zeolite, the diffusion coefficient was 7.8×10^{-18} m^2/s. Modification of the zeolite with 3.3 wt% Sb_2O_3 did not influence the diffusivity, which indicates that at this loading the modification with Sb_2O_3 did not influence the size of the pore openings or block parts of the pores. In contrast, at antimony oxide loading between 6.5 and 10.2 wt% a strong decrease in diffusion coefficients from 3.9×10^{-18} to 6.6×10^{-19} m^2/s was observed, which clearly indicates a narrowing of the pore entrances or blocking of a fraction of pores of the zeolite.

3.3. Catalytic activity

The activity and selectivity of the parent and Sb_2O_3-modified zeolites for toluene disproportionation are compared in Fig. 10. For the parent zeolite the ratio between

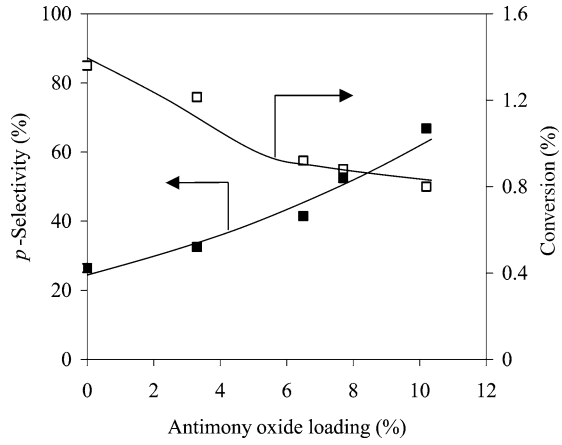

Fig. 10. Activity and selectivity of the modified zeolites for toluene disproportionation at 773 K.

the xylene isomers was close to thermodynamic equilibrium even under the differential conditions employed. After modification with Sb_2O_3 the *para*-selectivity increased from 33% (3.3 wt% Sb_2O_3) to 68% (10.2 wt% Sb_2O_3). The activity of the catalyst with the highest Sb_2O_3 loading (10.2 wt%), however, decreased by 41% compared with the unmodified zeolite.

4. Discussion

4.1. Dispersion of antimony oxide on the zeolite

Metal oxides and salts can be dispersed over different supports, such as Al_2O_3, SiO_2, TiO_2, ZrO_2, and zeolites, by solid-state reactions [19]. After the solid-state reaction of Sb_2O_3 with HZSM-5, crystalline antimony oxide phases were not detected by XRD even for samples with a Sb_2O_3 loading up to 10.2 wt%, which indicates an effective dispersion of Sb_2O_3 on the zeolite. Raman spectra of the physical mixture of antimony oxide and the zeolite calcined at different temperatures showed that the transformation of crystalline Sb_2O_3 into highly dispersed phases was competed at 723 K. In agreement with Raman results in situ IR spectroscopy revealed that the concentration of hydroxyl groups started to decrease at temperatures above 643 K due to the solid-state reaction between Sb_2O_3 and the zeolite. In principle, dispersion of metal oxides/salts occurs via surface diffusion. The dispersion of a metal oxide typically starts at temperatures above its Tammann temperature [38–40], which is approximately equal to half of the melting point of the oxide. For Sb_2O_3 over HZSM-5 the dispersion by solid-state reaction, however, started at temperatures above 643 K, which is substantially higher than the Tammann temperature of Sb_2O_3 (464 K). Note that during temperature-programmed desorption of H_2O, the dehydration of the zeolite occurred at approximately 600 K, which indicates that the solid-state reaction of Sb_2O_3 proceeds with the hydroxyl groups of the zeolite. Therefore, dehydration of the zeolite is necessary to generate active hydroxyl groups, as the interaction between the oxide and hydroxyl groups of the zeolite appears to be the driving force for the dispersion of Sb_2O_3. Significant loss of Sb_2O_3 (about 50% of the total amount used) occurring during the sample preparation by solid-state reaction (see Table 1) indicates that the transport of Sb_2O_3 via the vapor phase is possible at lower temperatures ($\sim$ 600 K), although the sublimation temperature of Sb_2O_3 is 1425 K. Therefore, we speculate that this process may also partially contribute to the dispersion of Sb_2O_3 over the zeolite.

After modification of the zeolites with antimony oxide, a marked decrease in the intensity of the silanol and bridging hydroxyl groups was observed. This indicates that antimony oxide strongly interacts not only with the bridging hydroxyl groups, but also with the silanol groups. Due to the weakly basic character of Sb_2O_3, the interaction of Sb_2O_3 with the accessible bridging hydroxyl groups (Brønsted acid sites)

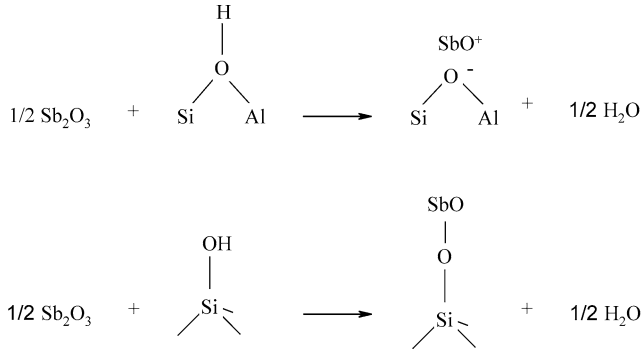

Scheme 1. Solid-state reaction of Sb_2O_3 with hydroxyl groups of HZSM-5 zeolite.

of the zeolite occurs via the formation of SbO^+ species, which act as charge compensating species, and, therefore, leads to partial removal of the acid sites. Due to the weakly acidic character of the SiOH groups the interaction of antimony oxide with the silanol groups is speculated to involve more covalent bonds. The surface reactions are depicted in Scheme 1. Note that the decrease in the concentration of SiOHAl groups after modification was independent of Sb_2O_3 loading. Moreover, with increasing Sb_2O_3 loading the accessible bridging hydroxyl groups were passivated before the reaction of Sb_2O_3 with the SiOH groups, which indicates that antimony oxide preferentially interacts with the bridging hydroxyl groups, because of their stronger acidity. Additionally, the concentration of Lewis acid sites decreased after modification, which reveals that antimony oxide also reacts with EFAL species. Similar to the interaction of antimony oxide with Brønsted acid sites, the decrease in concentration of Lewis acid sites was independent of Sb_2O_3 loading and, moreover, the accessible Lewis acid sites were observed to react with Sb_2O_3 before the removal of silanol groups was competed.

4.2. Influences of modification on the structural properties of the zeolite

Comparison of pore volumes before and after modification showed that the pore volume of the zeolite decreased after modification with 3.3 wt% Sb_2O_3 (see Table 1), which resulted from penetration of a small amount of antimony oxide into the pores of the zeolite. At higher Sb_2O_3 loading a further decrease in pore volume was not observed, which indicates that the deposition of Sb_2O_3 occurs primarily on the external surface. Note that a partial collapse of the zeolite framework structure after the modification can be excluded.

Adsorption of DTBPy indicated that after modification with 3.3 wt% Sb_2O_3 all externally accessible acid sites were removed by the reaction of Sb_2O_3 with accessible bridging hydroxyl groups. The decrease in concentration of Brønsted acid sites after modification (determined by IR spectroscopy and sorption of pyridine) was 50%, while DTBPy adsorption indicated that only 28% of the Brønsted acid sites were located in the pore mouth region of the parent zeolite [36]

(see Table 2). Therefore, antimony oxide not only interacts with Brønsted acid sites located in the pore mouth region, but also penetrates into the zeolite pores. The changes in the concentrations of Lewis and Brønsted acid sites were not a function of Sb_2O_3 loading, while the concentration of silanol groups continuously decreased with increasing antimony oxide loading (see Table 3). This clearly indicates that Sb_2O_3 interacts preferentially with the strongly acidic Brønsted and Lewis acid sites. After all strong acid sites accessible for Sb_2O_3 are passivated, antimony oxide is dispersed on the external surface of the zeolite crystals. Considering that the pore volume of SbZ4 remains identical to that of SbZ1, while the concentration of SiOH groups decreases from 60 to 98% we speculate that antimony oxide is polymerized on the external surface and in the pore mouth region of the zeolite at high Sb_2O_3 loadings.

The results of *o*-xylene adsorption support these conclusions. At low antimony oxide loading (3.3 wt%) the amount of *o*-xylene adsorbed decreased markedly compared with the parent zeolite; the diffusivity, however, remained unchanged. With increasing antimony oxide loading, *o*-xylene uptake did not decrease further, while diffusivity of *o*-xylene into the pores was strongly retarded. This indicates that at low Sb_2O_3 loading strong acid sites located in the pore mouth region and inside the pores are primarily passivated, which leads to reduction of the pore volume. SbO^+ species resulting from the reaction of Sb_2O_3 with the acid sites located in the pore mouth region are too small to influence the pore openings of the modified zeolite and the diffusivity of *o*-xylene. At higher Sb_2O_3 loading, Sb_2O_3 is polymerized on the external surface and in the pore mouth region which leads to a further narrowing of the pore openings and imposes a hindrance to the diffusion of molecules, i.e., antimony oxide or *o*-xylene, into the pores of the zeolite.

The solid-state reaction of antimony oxide with the zeolite was shown to occur via a combined surface and vapor diffusion mechanism. Antimony oxide diffuses in Sb_4O_6 subunits with a kinetic diameter of approximately 0.76 nm [41,42]. As these subunits are larger than the pore diameter of HZSM-5 zeolite, the diffusion of antimony oxide into the pores of the zeolite is sterically hindered, and therefore, only SiOHAl groups located in the pore mouth region are accessible. However, after modification a significantly higher concentration of Brønsted acid sites (50%) was found to be passivated compared with the concentration of externally accessible Brønsted acid sites (28%), which indicates that acid sites located inside the pores of the zeolite also participate in the solid-state reaction. This suggests that the Sb_4O_6 subunits are partially decomposed during the solid-state reaction of antimony oxide with the hydroxyl groups located on the external surface and in the pore mouth region of the zeolite. Smaller antimony oxide clusters formed subsequently enter into the zeolite pores and react with the bridging hydroxyl groups located in the pores of the zeolite.

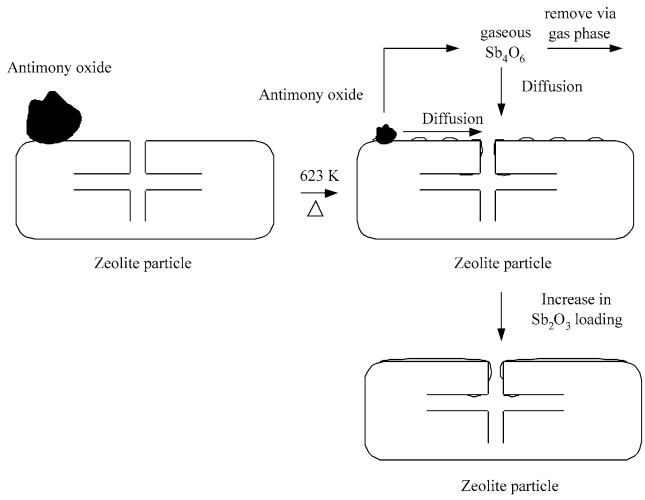

Scheme 2. Model of the dispersion of Sb_2O_3 in the pores and the external surface of the zeolite.

Based on the reactions described, the dispersion of antimony oxide during the solid-state reaction on the zeolite is depicted in Scheme 2. At low Sb_2O_3 loading, antimony oxide reacts with the bridging hydroxyl groups, nonframework Al oxide species, and silanol groups via surface and vapor diffusion. This interaction results in the complete passivation of externally accessible acid sites and the removal of Brønsted and Lewis acid sites by 50 and 20%, respectively. Most antimony oxide is located on the external surface and in the pore mouth region of the zeolite and only a minor amount of antimony oxide penetrates into the pores of the zeolite. Note that the reaction of antimony oxide with the bridging hydroxyl groups located in the pore mouth region of the zeolite slightly narrows the pore openings of the zeolite. This modification, however, is insufficient to influence *o*-xylene diffusivity. At higher Sb_2O_3 loadings, antimony oxide simultaneously reacts with the silanol groups and polymerizes on the external surface and in the pore mouths. This leads to narrowing/blocking of pore openings and induces considerable constraints for *o*-xylene diffusion.

4.3. Influence of modification on the activity and selectivity of the zeolites for toluene disproportionation

The activity and selectivity of HZSM-5 zeolites for toluene disproportionation are generally controlled by the concentration and location of Brønsted acid sites [43] and the dimensions of the pores, which can be adjusted by post-synthetic modifications. Narrowing of the pore openings of the zeolite lowers the diffusivity of *o*- and *m*-xylene, which typically leads to a strongly enhanced shape selectivity to *para*-product in the toluene disproportionation [2,36]. After modification with 3.3 wt% Sb_2O_3 the activity of toluene disproportionation decreased by 15% compared with the parent zeolite, which is directly related to the lower concentration of Brønsted acid sites of SbZ1. The enhanced *para*-selectivity of this catalyst is concluded to result pri-

marily from the passivation of the unselective Brønsted acid sites, as the modification only leads to a minor narrowing of the pore openings of SbZ1. Our previous study [44] showed that introducing acid sites onto the external surface of the zeolite decreased the *para*-selectivity for toluene disproportionation. Therefore, the passivation of unselective acid sites suppresses secondary isomerization reactions of *p*-xylene, generated inside the pores, to other isomers and thus enhances *p*-selectivity. At higher antimony oxide loading, a marked increase in *para*-selectivity up to 60% was observed at the expense of activity compared with the unmodified HZSM-5. The enhanced *para*-selectivity for samples with higher Sb_2O_3 loading could be attributed to further pore narrowing, which constrains the diffusion of *o*- and *m*-xylene isomers, as the concentration of Brønsted acid sites remains constant at higher antimony oxide loading. Therefore, the decrease in activity of HZSM-5 catalysts modified with higher Sb_2O_3 loadings results from mass transfer limitations on the products in the narrowed pores of the modified zeolites.

5. Conclusions

Antimony oxide can be dispersed on the surface and inside the pores of zeolites by solid-state reactions at elevated temperatures via a surface and vapor diffusion process. Crystalline antimony oxide phases were not detected even at antimony oxide loadings up to 10.2 wt%. In situ Raman and IR spectroscopy indicated that the solid-state reaction commenced at 623 K and was complete at 723 K. During the solid-state reaction antimony oxide clusters reacted with the silanol and bridging hydroxyl groups and with extra-framework Al oxide species of the zeolite. A small amount of antimony oxide penetrated into the pores of the zeolite and reacted with the bridging hydroxyl groups. The large fraction of antimony oxide, however, was located on the external surface of the zeolite crystals and led to a narrowing of the pore openings of the zeolite, which suppressed the further penetration of antimony oxide into the pores of the zeolite. The modification of HZSM-5 zeolite with antimony oxide led to the complete passivation of unselective Brønsted acid sites at low Sb_2O_3 loadings and to narrowing of the pores at higher Sb_2O_3 loadings. Both effects resulted in enhanced shape selectivity to *p*-xylene in the toluene disproportionation reaction, but also led to lower activity due to the lower concentration of Brønsted acid sites and the generation of mass transfer limitations in the Sb_2O_3-modified zeolites.

Compared with CVD and CLD with ethoxysilanes, modification with Sb_2O_3 passiviates the acid sites, which is followed by pore narrowing. Therefore, the influence of passivation of unselective acid sites and pore narrowing can be differentiated, while CLD and CVD typically remove unselective acid sites and narrow the pore mouth at the same time. Also, it is possible to completely remove all Brønsted acid sites by solid-state reaction with Sb_2O_3, while it is very difficult to completely remove unselective acid sites by CLD or CVD, even by multicycle modification [36].

Acknowledgments

The authors thank M. Brandmair for the Raman measurements and J.-O. Barth and R.Q. Su for the ^{27}Al MAS NMR measurements. Financial support from the Bayerische Forschungsverbund Katalyse (FORKAT II) and Süd-Chemie AG is gratefully acknowledged.

References

[1] S.M. Csicsery, Zeolites 4 (1984) 202.
[2] T. Tsai, S. Liu, I. Wang, Appl. Catal. A 181 (1999) 355.
[3] D.H. Olson, W.O. Haag, Catalytic Materials, in: ACS Symposium Series, Am. Chem. Society, Washington, DC, 1984, p. 248.
[4] U. Kürschner, H.G. Jerschkewitz, E. Schreier, J. Völter, Appl. Catal. 57 (1990) 167.
[5] J. Cejka, B. Wichterlova, Catal. Rev. 44 (2002) 375.
[6] L.Y. Fang, S.B. Liu, I. Wang, J. Catal. 185 (1999) 33.
[7] J. Kim, A. Ishida, M. Okajima, M. Niwa, J. Catal. 161 (1996) 387.
[8] H.A. Begum, N. Katada, M. Niwa, Micropor. Mesopor. Mater. 46 (2001) 13.
[9] P. Tynjala, T.T. Pakkanen, J. Mol. Catal. A 122 (1997) 159.
[10] W.W. Kaeding, S.A. Butter, J. Catal. 61 (1980) 155.
[11] W.W. Kaeding, C. Chu, L.B. Young, B. Weinstein, S.A. Butter, J. Catal. 67 (1981) 159.
[12] W.W. Kaeding, L.B. Young, C.C. Chu, J. Catal. 89 (1984) 267.
[13] L.B. Young, S.A. Butter, W.W. Kaeding, J. Catal. 76 (1982) 418.
[14] B. Delmon, P.A. Jacobs, G. Poncelet, Preparation of Catalyst, Elsevier, Amsterdam, 1976.
[15] D.W. Breck, Zeolite Molecular Sieves, Wiley, New York, 1974.
[16] S. Zheng, H. Heydenrych, P. Röger, A. Jentys, J.A. Lercher, Stud. Surf. Sci. Catal. 135 (2001) 214.
[17] Y.H. Yue, Y. Tang, Y. Liu, Z. Gao, Ind. Eng. Chem. Res. 35 (1996) 430.
[18] H.G. Karge, K.B. Hermann, Stud. Surf. Sci. Catal. 69 (1991) 43.
[19] Y. Xie, Y. Tang, Adv. Catal. 37 (1990) 1.
[20] G. Kinger, A. Lugstein, R. Swagera, M. Ebel, A. Jentys, H. Vinek, Micropor. Mesopor. Mater. 39 (2000) 307.
[21] A. Lugstein, A. Jentys, H. Vinek, Appl. Catal. A 166 (1998) 29.
[22] R.W. Borry, E.C. Lu, Y.H. Kim, A. Huffsmith, J.A. Reimer, E. Iglesia, J. Phys. Chem. B 103 (1999) 5787.
[23] W. Ding, G.D. Meitzner, E. Iglesia, J. Catal. 206 (2002) 14.
[24] F. Xiao, S. Zheng, J. Sun, R. Yu, S. Qiu, R. Xu, J. Catal. 176 (1998) 474.
[25] G.Y. Lee, J.C. Zhao, Petrochem. Technol. (Chin.) 16 (1987) 266.
[26] G. Mirth, J. Cejka, J.A. Lercher, J. Catal. 139 (1993) 24.
[27] G. Mirth, J.A. Lercher, J. Catal. 147 (1994) 199.
[28] J. Kärger, D.M. Ruthven, Diffusion in Zeolite and Other Micro-Porous Solids, Wiley, New York, 1992.
[29] C. Cavalcante, D. Ruthven, Ind. Eng. Chem. Res. 34 (1995) 185.
[30] G. Mestl, J. Mol. Catal. A 158 (2000) 45.
[31] M.B. Sayed, R.A. Kydd, R.P. Cooney, J. Catal. 88 (1984) 137.
[32] V.P. Glazunov, S.E. Odinokov, Spectrochim. Acta A 38 (1982) 399.
[33] C.A. Emeis, J. Catal. 141 (1993) 347.
[34] H. Knözinger, H. Krietenbrink, P. Ratnasamy, J. Catal. 48 (1977) 436.
[35] A. Corma, V. Fornes, L. Forni, F. Marquez, J. Martinez-Triguero, D. Moscotti, J. Catal. 179 (1998) 451.

[36] S. Zheng, H.R. Heydenrych, A. Jentys, J.A. Lercher, J. Phys. Chem. B 106 (2002) 9552.
[37] R. Roque-Malherbe, R. Wendelbo, A. Mifsud, A. Corma, J. Phys. Chem. 99 (1995) 14064.
[38] H. Knözinger, E. Taglauer, in: G. Ertl, H. Knözinger, J. Weitkamp (Eds.), Handbook of Heterogeneous Catalysis, Vol. 1, Wiley–VCH, Weinheim, 1997, p. 216.
[39] H. Knözinger, E. Taglauer, in: J.J. Spivey (Ed.), Catalysis, Vol. 10, Royal Society of Chemistry, Cambridge, UK, 1993, p. 1.
[40] G. Mestl, H. Knözinger, Langmuir 14 (1998) 3964.
[41] N.C. Norman (Ed.), Chemistry of Arsenic Antimony and Bismuth, Blackie Academic and Professional, London, 1992.
[42] J. Spengler, F. Anderle, E. Bosch, R.K. Grasselli, B. Pillep, P. Behrens, O.B. Lapina, A.A. Shubin, H.J. Eberle, H. Knözinger, J. Phys. Chem. B 105 (2001) 10772.
[43] H. Vinek, J.A. Lercher, J. Mol. Catal. 64 (1991) 23.
[44] S. Zheng, H.R. Heydenrych, H.P. Röger, A. Jentys, J.A. Lercher, Top. Catal. 22 (2003) 101.